International Journal of Advances in Electrical Engineering

E-ISSN: 2708-4582
P-ISSN: 2708-4574
IJAEE 2025; 6(1): 36-44

www.electricaltechjournal.com
Received: 01-01-2025
Accepted: 05-02-2025

D Sahitya Devi
Assistant Professor, Department of EEE, Usha Rama College of Engineering and Technology, Telaprolu, Andhra Pradesh, India

V Pardha Sai
UG Scholar, Department of EEE, Usha Rama College of Engineering and Technology, Telaprolu, Andhra Pradesh, India

M Jagadeesh Naidu
UG Scholar, Department of EEE, Usha Rama College of Engineering and Technology, Telaprolu, Andhra Pradesh, India

Correspondence
D Sahitya Devi
Assistant Professor, Department of EEE, Usha Rama College of Engineering and Technology, Telaprolu, Andhra Pradesh, India

Hybrid E-rickshaw powered by solar PV and regenerative braking with sensor less control

D Sahitya Devi, V Pardha Sai and M Jagadeesh Naidu

DOI: https://www.doi.org/10.22271/27084574.2025.v6.i1a.84

Abstract
A novel drivetrain design of a solar-powered e-rickshaw with the controller. Hall-Effect position sensor less brushless DC (BLDC) motor drive often suffers from delayed commutation at high speed and even at low speed, conventional control does not work well due to low magnitude of back EMF. Here, the proposed sensor less control with commutation error compensation is implemented, which drives the motor over the entire range. A simple commutation error compensation algorithm is designed to detect the freewheeling pulses, reducing the control complexity for low-cost EV application and eliminating low pass filter requirement. Moreover, a zero-crossing detection (ZCD) algorithm is suggested, which inherently compensates the delay and removes the need of any additional phase compensator. A fixed delay digital filter is used to eliminate any unwanted spikes in ZCD circuit. For effective MPPT control, a modified Landsman converter is used, which provides ripple-free current at output and reduces the requirement of ripple filter at front end. The BLDC motor drive is capable of energy regeneration, which reduces the range anxiety for EV. The solar energy and the battery ensure that the vehicle never runs out of power irrespective of the climate conditions. The average distance covered by the vehicle on a single charge is improved.

Keywords: Solar-powered e-rickshaw, sensor less brushless DC (BLDC) motor drive, zero-crossing detection (ZCD), landsman converter, maximum power point tracking (MPPT)

1. Introduction
Electric rickshaws are among the most prevalent electric vehicles (EVs) in India and form a vital segment of the country's public transport infrastructure. However, limited battery capacity poses a significant challenge by restricting the driving range. Implementing regenerative braking—where the kinetic energy of the vehicle is converted back into electrical energy and fed to the battery—can improve the battery's state of charge (SoC). This approach enhances energy efficiency and extends operating range without needing to increase battery size, which would otherwise raise system weight and cost Brushless DC (BLDC) motors are gaining widespread attention in electric vehicle applications due to their high energy density and simplified control architecture. Traditional BLDC motor control systems rely on three Hall-effect sensors mounted on the stator to detect rotor positions, requiring additional signal processing to generate six distinct position signals. However, these sensors are vulnerable in harsh environments and can lead to reliability issues in EVs. Speed control of the BLDC motor is generally achieved using a Proportional-Integral (PI) controller alongside PWM signal generation. For enhanced performance under varying load conditions, a PID controller is implemented to ensure more accurate and robust speed regulation.
One key issue affecting high-speed applications of BLDC motors is commutation error, which significantly degrades system efficiency. These errors are difficult to eliminate due to various non-ideal factors influencing the accuracy of commutation. To address this, a sensor-less control method using third-harmonic voltage compensation is proposed. This technique not only reduces commutation errors but also improves the overall system performance and reliability.
Ensuring steady output across varying operational conditions necessitates the use of a reliable motor drive system connected to an appropriate converter configuration. Power electronic converters play a critical role in managing the energy flow from the source. These converters—comprising semiconductor devices suitable for both low-and high-power

applications—include various types like DC-DC, AC-DC, and AC-AC converters, designed to optimize energy conversion. Commonly used topologies such as boost and buck-boost converters are cost-effective and simple, making them suitable where the load is directly connected. However, they often fall short in high step-up voltage applications due to limited voltage gain and associated inefficiencies.

To overcome these challenges, the Landsman converter is introduced as a superior alternative to SEPIC, ZETA, and Cuk converters. It offers better performance with fewer components, addressing issues like low efficiency, bulky capacitors, and excessive passive elements. Effective control of the Landsman converter is crucial to achieving high voltage gain, and this is done through various control strategies including PWM, PI, and PID controllers that generate accurate gate signals for the power switches. A fuzzy-PID controller is adopted to improve the DC link voltage stability, reduce settling time, and ensure a reliable power supply to the three-level voltage source converter (VSC).

Furthermore, the integration of a fuzzy-PID controller with a back-EMF-based BLDC motor control using Indirect Field-Oriented Control (IFOC) enhances overall system stability. To extract maximum power from a photovoltaic (PV) source that feeds the Landsman converter-driven BLDC motor, a Maximum Power Point Tracking (MPPT) algorithm based on Incremental Conductance (IncCond) is employed. Comparative analysis reveals that the proposed system demonstrates improved DC link voltage regulation and faster dynamic response compared to conventional setups.

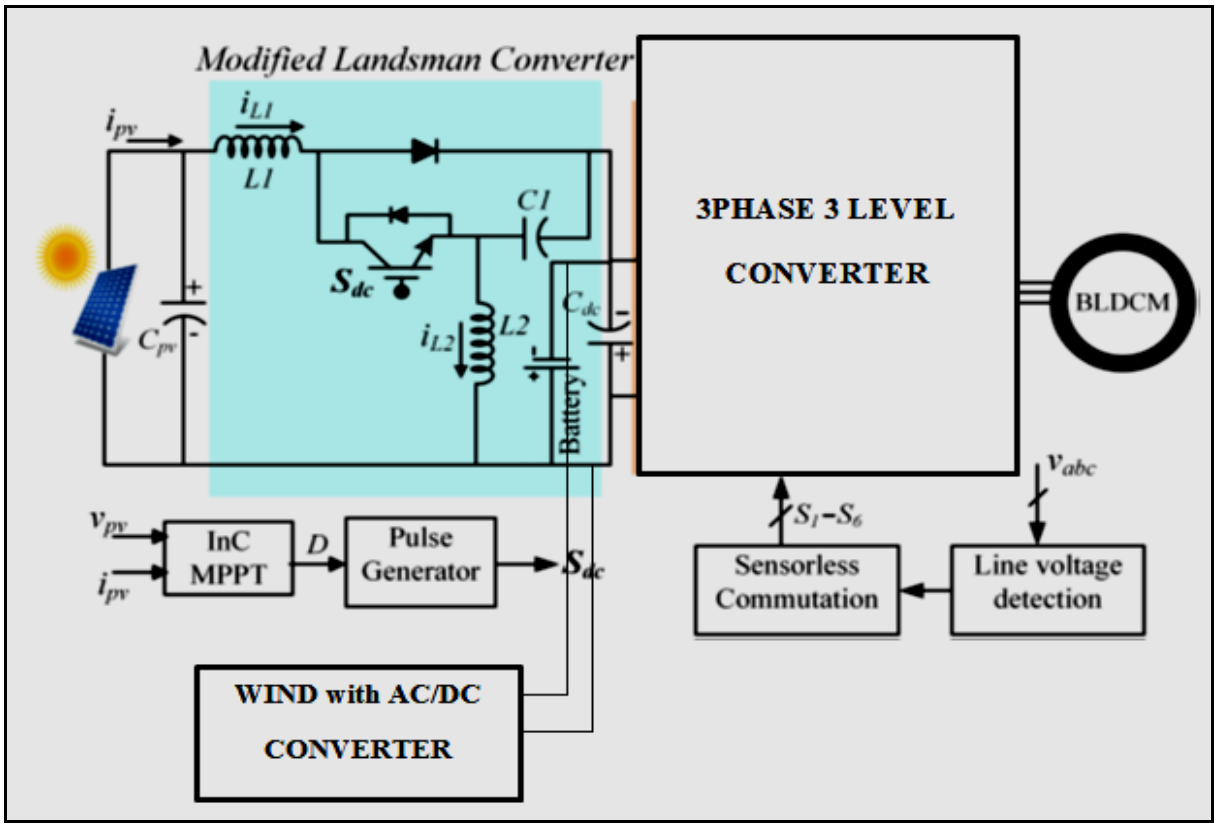

Fig 1: Block Diagram of Proposed Converter

2. Proposed System

In the proposed system, illustrated in Figure 1, a photovoltaic (PV) source supplies direct current to a brushless DC (BLDC) motor drive. The overall system configuration includes a three-level voltage source inverter (VSI), a Landsman converter, a single-diode PV array, a wind energy-based AC/DC converter, and the BLDC motor. The Landsman converter (LC) is responsible for achieving high voltage gain, which is then supplied to the VSI that drives the BLDC motor. The Fuzzy-PID control strategy is implemented to regulate the LC, aiming to enhance voltage gain and minimize the output voltage settling time. Additionally, a sensor-less control technique is utilized to manage the BLDC motor's speed and effectively reduce torque ripple.

3. Modelling of PV system

The Photovoltaic (PV) array block models a group of interconnected PV modules. Within the array, each string consists of modules connected in series, while multiple strings are linked in parallel to form the complete setup. This block simulates the current-voltage (I-V) characteristics of the modules, which vary with changes in irradiance and temperature. It utilizes a five-parameter model comprising a light-generated current source (IL), a diode characterized by saturation current (I_0) and ideality factor (nI), along with a series resistance (Rs) and a shunt resistance (Rsh).

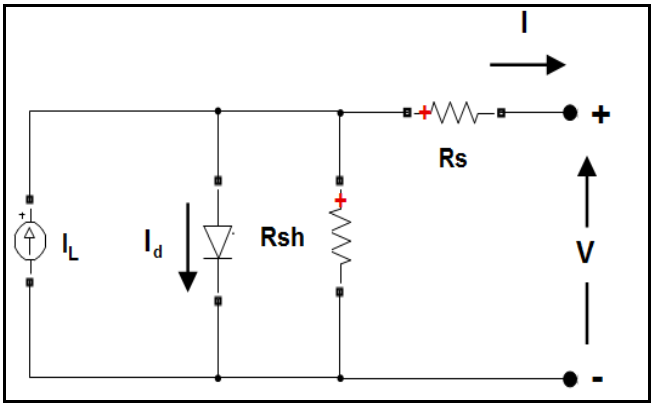

Fig 2: Single Diagram of PV System

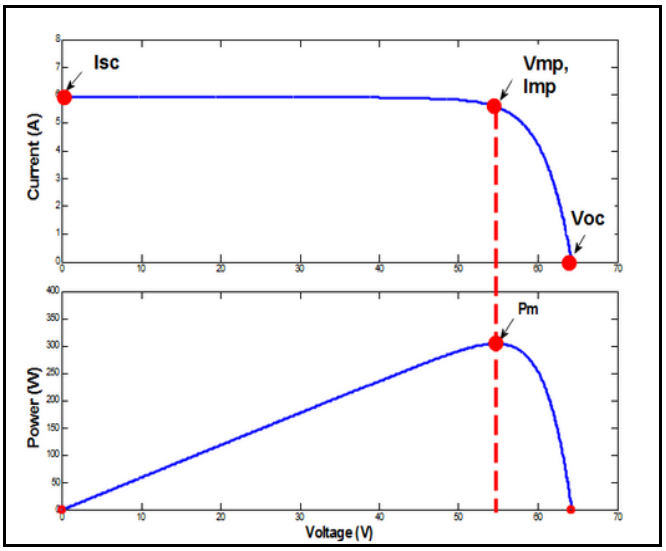

Fig 3: PV characteristics

The equations define the current-voltage (I-V) behavior of an individual PV module based on its diode characteristics.

$$I_d = I_0\left[\exp\left(\frac{V_d}{V_T}\right) - 1\right]$$

$$V_T = \frac{kT}{q} \times nI \times Ncell \quad (1)$$

The diode current-voltage (I-V) characteristics for a single PV module are defined by standard semiconductor equations. In these equations: *Id* represents the diode current, Vd is the diode voltage, *Io* denotes the diode saturation current, *nI* is the diode ideality factor, k is the Boltzmann constant, q represents the electronic charge, T stands for the cell temperature, and Ncell is the number of series-connected cells within the module.

The electric vehicle (EV) system is powered by a high-efficiency solar panel rated at a peak power of 380 W. The design of the solar PV array and the associated power converter is based on key parameters such as the panel's open-circuit voltage and short-circuit current. Specifically, an open-circuit voltage of 70 V and a short-circuit current of 9.36 A are selected. When operating under maximum power point tracking (MPPT) conditions, the panel exhibits a voltage Vmp of approximately 47 V. Accordingly, the current at maximum power point, Imp, is calculated as 380 W / 47 V ≈ 8 A.

The MPPT algorithm used in the system is based on the incremental conductance method. It locates the maximum power point (MPP) by equating the incremental conductance (*ΔIpv / ΔVpv*) with the instantaneous conductance (*Ipv / Vpv*). This algorithm dynamically adjusts the duty cycle of the modified Landsman converter to maintain optimal power extraction from the PV source.

Gate pulses required for the converter's operation are generated by a high-frequency pulse generator. The system is optimized for ideal solar irradiance conditions during planning. Additionally, the enhanced buck-boost behaviour of the Landsman converter allows it to effectively manage variations in sunlight, including partial shading. This approach helps mitigate power losses, potentially reducing shading-induced losses by up to 10%.

4. Designing of landsman converter

The Landsman Converter (LC) is a type of DC-DC converter designed to enhance power extraction from the photovoltaic (PV) source. Its performance in Continuous Conduction Mode (CCM) is influenced by variations in solar irradiance. The proposed LC improves the voltage supply to the brushless DC (BLDC) motor, ensuring reduced voltage settling time and enhancing motor operation. It effectively regulates the output voltage from the PV array, contributing to a more stable, efficient, and quieter BLDC motor performance.

By controlling the DC bus voltage, the LC enables higher voltage gain in the overall system. The converter architecture includes two inductors (L1 and L2), a switching device (Sdc), and a capacitor (C1). The LC's input is directly connected to the output of the solar panel, while its output is linked to a DC link capacitor (Cdc), which stabilizes the voltage supplied to downstream components.

For this setup, the PV panel's voltage and current ratings are configured as Vpv = Vmp = 47 V and Ipv = Imp = 8.11 A. Given this, the current flowing through the input inductor L1 is equal to the PV current, i.e., IL1 = 8.11 A. Based on these values, the duty ratio for operating the DC-DC converter can be determined as follows:

$$D = \frac{V_{dc}}{V_{dc} + V_{pv}} = \frac{48}{48 + 46.8} = 0.506 \quad (2)$$

where Vdc and Vpv represent the voltages of the DC bus and the PV panel output, respectively. To calculate the current flowing through the DC link capacitor at maximum power output, the following formula is applied:

$$I_{dc} = \frac{P_{mp}}{V_{dc}} = \frac{380}{48} = 7.91A. \quad (3)$$

A switching frequency of 20 kHz is employed to generate PWM pulses for controlling the converter. The symbols IL1 and IL2 represent the currents flowing through inductors L1 and L2, respectively. While a small ripple is permissible in the circuit for the purpose of component sizing, the output voltage ripple is effectively minimized due to the use of a high-capacity DC bus capacitor. The design of this capacitor is further optimized by considering the minimum and maximum angular frequencies of the voltage source inverter (VSI). The detailed parameters used in designing the Landsman converter are summarized in Table I.

5. PID fuzzy controller

Unlike conventional control methods that rely on precise mathematical equations to describe system behavior, fuzzy logic utilizes linguistic terms to represent operational rules. In many complex systems, developing accurate mathematical models becomes infeasible, making traditional control strategies less effective. Fuzzy logic offers a practical alternative by using verbal descriptions to define the system's behavior, allowing for greater flexibility and adaptability. Fuzzy logic controllers are a type of symbolic controller designed to handle such complexity.

In this research, the proposed PV-based system incorporates both DC-DC and DC-AC converters, where each power switch (*S*) is controlled using a Fuzzy-PID controller. The control strategy integrates a fuzzy logic approach with conventional PID control to enhance performance. Specifically, a Fuzzy-PID controller is employed within a three-level converter topology and a brushless DC (BLDC) motor-driven photovoltaic system to achieve improved voltage gain and dynamic response.

Table 1: The detailed parameters used in designing the Landsman converter are summarized

Para-meter	Expression	Design data	Value
C_1	$\frac{D \times I_{dc}}{f_{sw} \times \Delta V_{dc}}$	D = 0.506 I_{dc}= 7.91 A V_{dc}= 48 V ΔV_{dc}=10% of V_{dc} f_{sw}=20 kHz	41.69 µF
L_1	$\frac{D \times I_{dc}}{8 \times f_{sw}^2 \times C_1 \times \Delta I_{L1}}$	D = 0.506 I_{dc}= 7.91 A f_{sw}=20 kHz I_{L1}= 8.11 A ΔI_{L1}= 5% of I_{L1} C_1=41.69 µF	73.98 µH
L_2	$\frac{D \times V_{mp}}{f_{sw} \times \Delta I_{L2}}$	D = 0.506 V_{mp}= 46.8 V f_{sw}=20 kHz I_{L2}= I_{mp} - I_{dc} ΔI_{L2}= 5% of I_{L2}	5.85 µH
C_{dc}	$\omega_h = 2 \times \pi \times f = \frac{2 \times \pi \times N_r \times P}{120}$ $\omega_l = 2 \times \pi \times f = \frac{2 \times \pi \times N \times P}{120}$ $C_h = \frac{I_{dc}}{6 \times \omega_h \times \Delta V_{dc}}$ $C_l = \frac{I_{dc}}{6 \times \omega_l \times \Delta V_{dc}}$	P=6 N_r=3000 rpm N=800 rpm I_{dc}= 7.91 A V_{dc}= 48 V ΔV_{dc}=10% of V_{dc}	C_h=306.88 µF C_l=1092.8 µF C_{dc}=1000 µF

Table 1

Even when the set points change, the proposed control system consistently provides the desired reference value. This control strategy incorporates both fuzzy logic and PID controllers. A traditional PID controller adjusts the system based on the proportional, integral, and derivative parameters to minimize oscillations and manage steady-state errors. In the suggested system, a Fuzzy-PID controller is employed to optimize the converter's switching signals, especially when the load and set points are dynamic.

The Fuzzy-PID controller uses fuzzy logic to determine the optimal values for the proportional (Kp), integral (Ki), and derivative (Kd) gains. The controller takes two inputs—error and the rate of change of error (delta error)—and generates three outputs corresponding to the Kp, Ki, and Kd values. By leveraging fuzzy logic, this controller reduces settling time and enhances overall system performance. The developed Fuzzy-PID controller improves the input voltage source for the voltage source inverter (VSI). The block diagram illustrating the proposed Fuzzy-PID controller architecture for the DC-DC Landsman converter is shown in Figure 4.

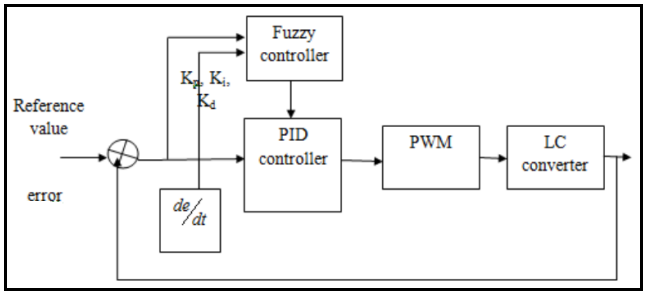

Fig 4: Fuzzy-PID controller Block Diagram

In the design of any fuzzy system, three key factors must be considered:

1. Fuzzy rules are
2. Membership functions are chosen and adjusted
3. Scaling factors are chosen in

Fuzzy logic, a mathematical approach, offers a novel method for enhancing the regulation of voltage, frequency, and current in variable-speed drives. In electric vehicle (EV) applications, fuzzy logic can address challenges arising from system non-linearity and its dynamic nature, which are difficult to manage using traditional control methods. These characteristics are inherent in the proposed control system.

The fuzzy logic membership functions in this system are divided into five categories, as shown in Figure 5, with five membership functions (MF) for both the input and output fuzzy sets. A Mamdani fuzzy inference system is employed to map two input variables to a single output variable. The two input variables are the error (e), which represents the difference between the desired (set-point) and measured value, and the change in error (d), which is used to denormalize the specific variables of a conventional control gain.

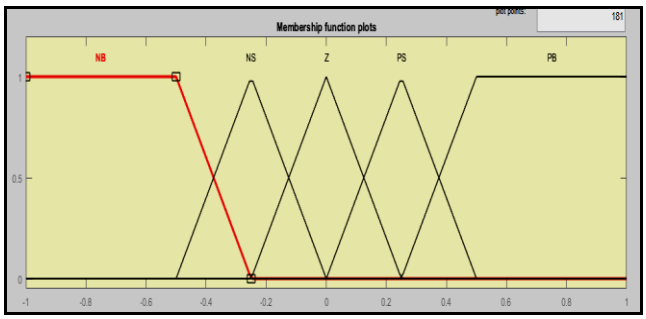

Fig 5: Membership function of FLC

Table 2: Fuzzy Rules

Δwe	NB	NS	Z	PS	PB
NB	NB	NB	NS	Z	PS
NS	NB	NS	Z	PS	Z
Z	NS	Z	PS	PS	PB
PB	Z	PS	PB	PB	PB

Rather than simply interpreting the fuzzy sets as NB (Negative Big), NS (Negative Small), Z (Zero), PS (Positive Small), and PB (Positive Big), this approach offers a method to improve the accuracy of continuous control rules through interpolation of the basic rule table. In this method, symmetric triangular membership functions (MFs) with equal bases and 50% overlap with adjacent MFs are used, except for the two outermost groups, where trapezoidal MFs are selected. By integrating this fuzzy controller into the outer loop and using the error signal and its variation as input signals, the system's performance can be enhanced, particularly for electric vehicle (EV) applications.

6. Simulation Implementation

The proposed Simulink model incorporates a Fuzzy-PID controller with a Landsman converter, where a BLDC motor is driven by renewable energy from a photovoltaic (PV) array. When the PV modules generate low energy, it is directed to the Landsman converter to regulate the high DC link voltage. The output DC voltage from the PV-fed converter is then supplied to the Voltage Source Inverter (VSI), which produces three-phase voltages for the operation of the BLDC motor. The primary Fuzzy-PID controller in this system is designed to regulate the DC link voltage response of the LC converter and reduce the settling time.

Figure 6 illustrates the Simulink model of the proposed system, showcasing how the controller manages the converter's performance. The Maximum Power Point Tracking (MPPT) algorithm is employed to ensure the generation of maximum possible power from the PV array.

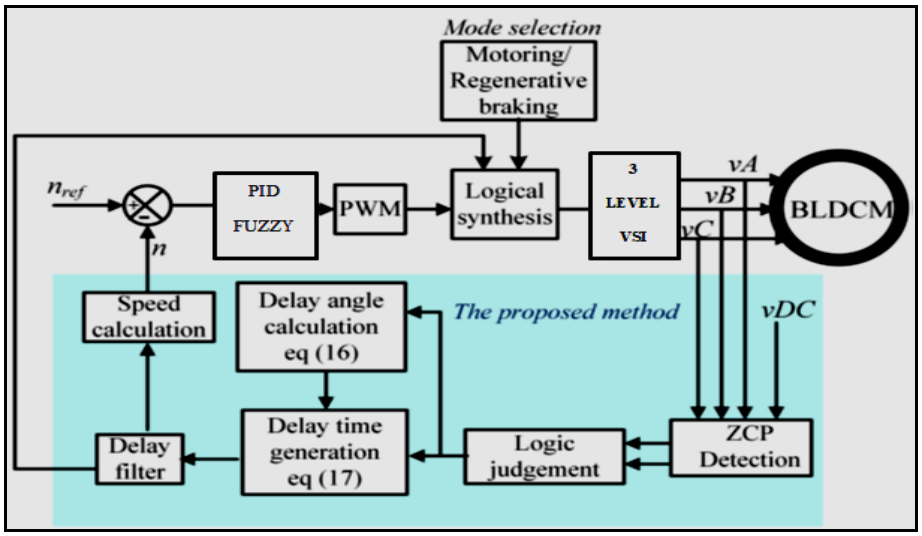

Fig 6: Proposed Simulink Diagram

The Hall Sensor (HC), which relies on hall signal measurements from the desired drive rotor angle, generates the switching signals for the system. The voltage and current of the brushless DC motor stator are estimated using a sensor-less back Electromotive Force (EMF) approach. This estimation enables control of the system's speed and torque. The rotor's position and speed are accurately observed using the proposed method.

The suggested cascaded multilevel inverter incorporates a PID-based control strategy to generate the necessary switching signals, helping to reduce harmonics in the carrier arrangement. The system is designed using a three-level inverter. Figure 7 shows the Simulink implementation of the proposed circuit, and the parameters for the system are detailed in Tables 3 and 4.

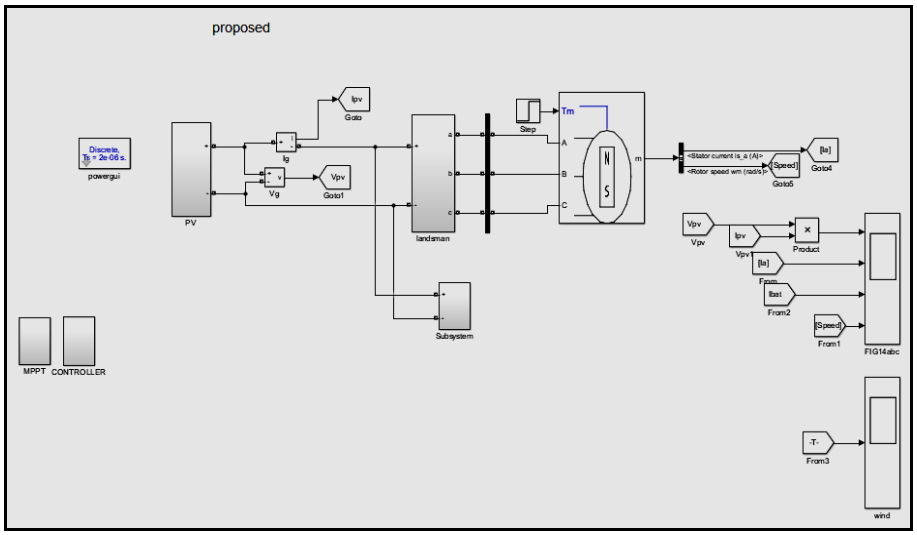

Fig 7: Simulink Implementation of Proposed Circuit

Table 3: System Parameters

Component of drive	Value
BLDC motor	48 V, 850 W (nominal), single speed, 7:1 gear arrangement
Solar-PV array	250 W (maximum)
Battery pack	Lithium-ion, 48 V, 100 Ah
Power converters	A 2-kW modified Landsman converter and A10 kW three-phase VSI

Table 4: BLDC Motor Specifications

BLDC motor parameter	Value
Stator per phase resistance, (Rph)	0.18 Ω
Stator per phase inductance, (L)	50 mH
Motor constant (Vpeak·L-L / krpm)	33.513
Motor torque constant (Nm/Apeak)	0.32
Pole pairs	2
Inertia (kg·m²)	0.02

7. Simulation Results

The proposed drive system will be thoroughly tested using an 850 W Permanent Magnet Brushless DC (PMBLDC) motor. Position sensor less control will be implemented under different loading conditions and speed variations. The experimental results and corresponding discussions are provided below.

7.1 Results of Solar PV System with MPPT Control

The input power to the drive is smoothly regulated according to the available solar irradiation. Power for the motor is provided simultaneously by the solar panel, battery, and wind energy, with the energy conversion handled by an AC-DC converter. Figure 8 illustrates that when solar irradiation decreases, the battery power increases to maintain a constant motor speed. Conversely, on sunny days, when solar irradiation is sufficient, power consumption from the battery decreases. Despite the variations in power sources, the motor speed remains consistent during both transient scenarios. A constant load torque of 1.4 Nm is applied throughout the process. A comparison of the converter's output power during a rapid load shift shows that the modified Landsman converter offers better stability, with reduced ripple and faster settling times.

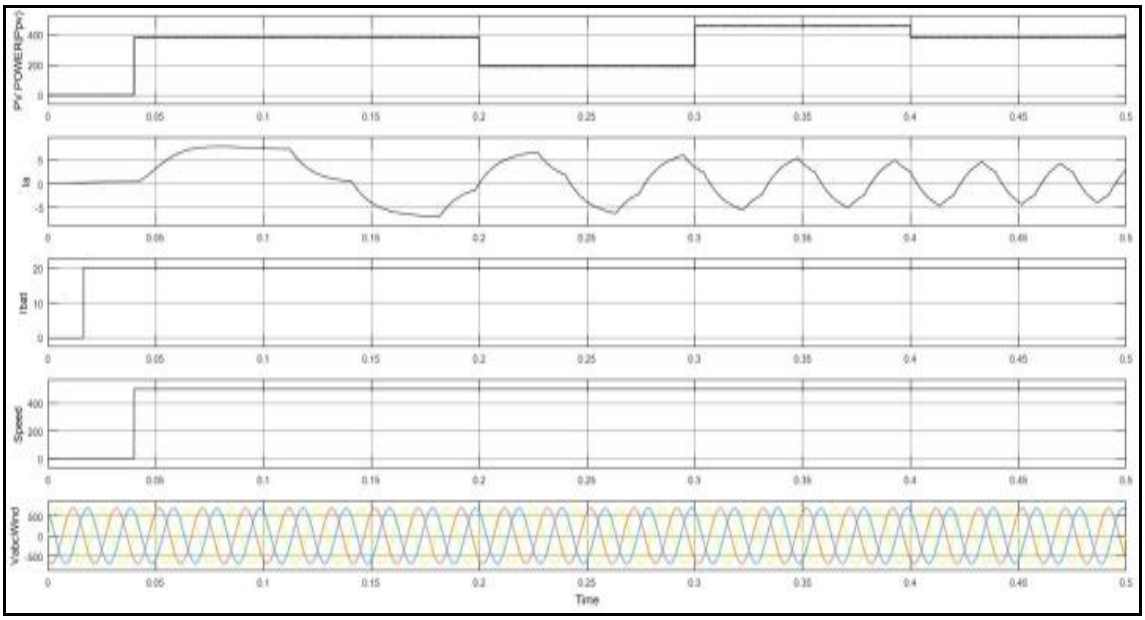

Fig 8: Pv Power, Stator Current, Battery Current Motor Speed, Wind Voltage

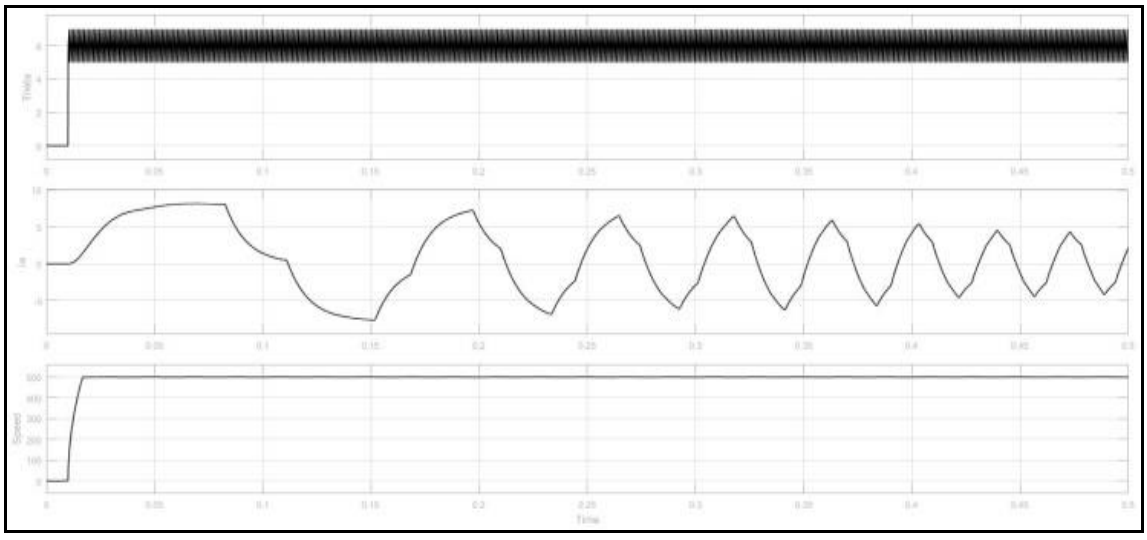

Fig 9: Theta, Ia, Speed

7.2 BLDC Motor Drive Performance with Position Sensorless

Figure 9 shows the rotor angle (Theta), stator currents, and speed of the proposed system under steady-state conditions. Once the rotor begins to accelerate, the sensor-less algorithm takes control. Initially, the rotor is aligned to a predetermined position by activating two phases using a specific commutation logic. To provide the high starting torque required by the electric vehicle (EV), the phase current is nearly double the rated current. In contrast to the LPF-based nonsensical control, which requires around 400 ms of forced acceleration, the proposed method transitions to sensor-less running mode in approximately 230 milliseconds. During startup, the load torque is set to 3 Nm. The current control ensures a smooth and quick start by preventing any current spikes during the initial phase.

7.3 At Different Speed Conditions

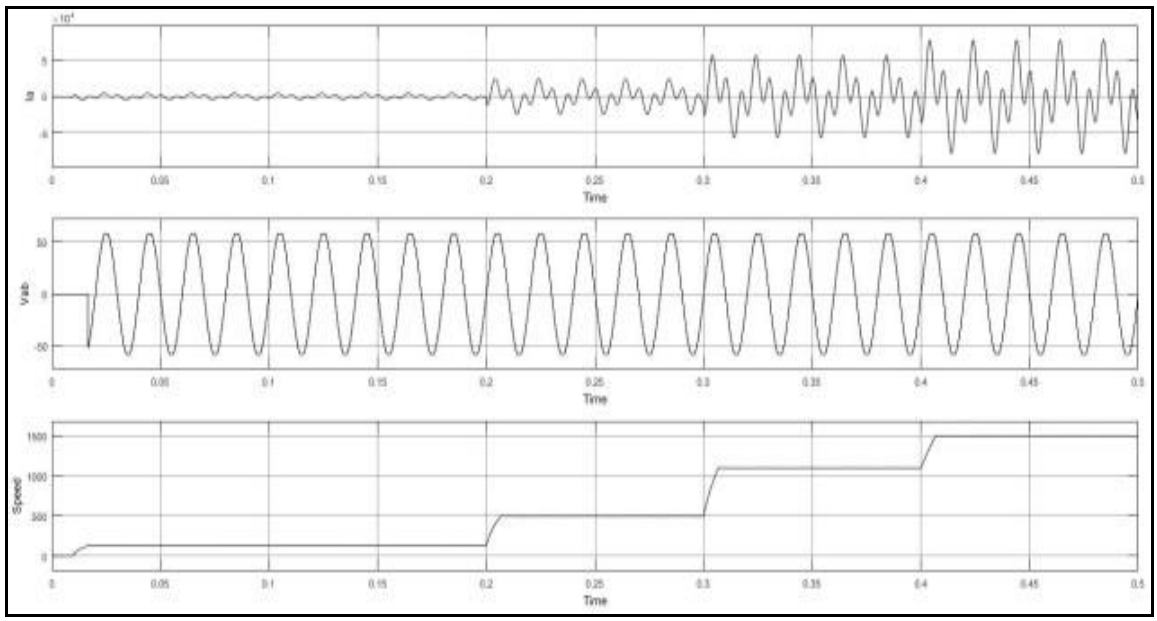

Fig 10: Performance of System under Different Speed Conditions at 130 rpm, 500 rpm, 1100 rpm

Figure 10 illustrates the effect of the proposed commutation error correction logic on phase current at different speeds. The suggested method is compared with the traditional LPF-based delay compensation logic for this EV application, showing a noticeable reduction in current ripple (ia). The current ripple increases at high speeds when using the proposed method, which can be attributed to imperfect Zero Crossing Points (ZCPs). Although the LPF-based method also accounts for delay, the current spikes observed during commutation are caused by an unbalanced DC link voltage and calculation delays in the software. The proposed method, however, maintains the integrity of the current profile and keeps the ripple under control. As a result, the suggested compensation technique eliminates current spikes and improves sensor-less commutation in the BLDC motor drive.

4. Performance under different load conditions

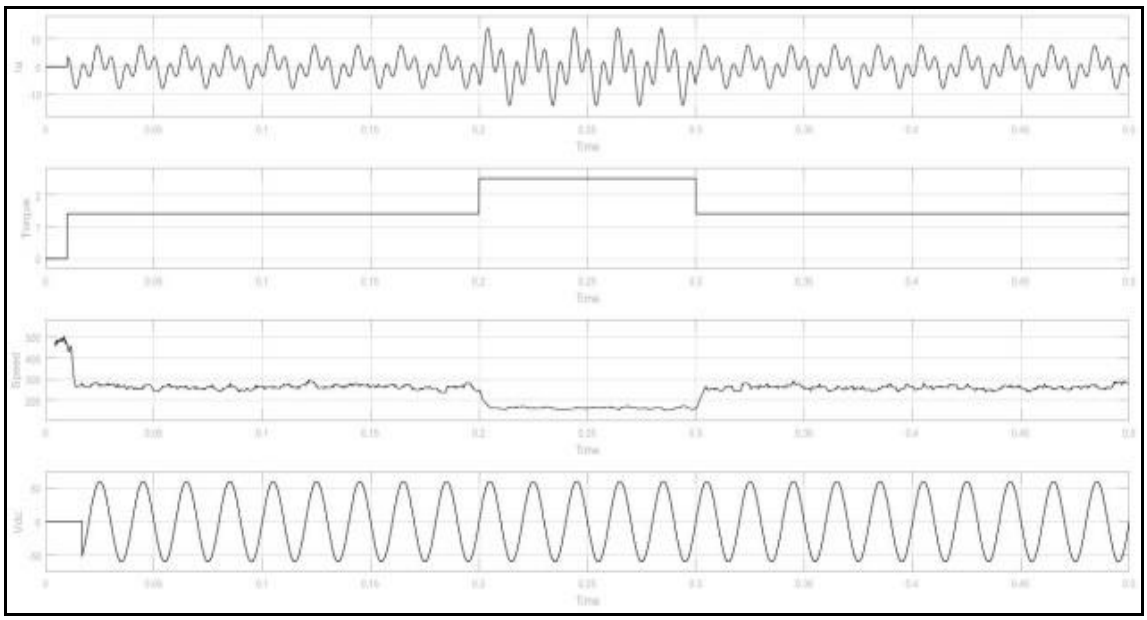

Fig 11: Ia, Torque, Speed, Vab

Figure 11 demonstrates the dynamic performance of the drive as the load changes. As the load increases to the rated 2.6 Nm, there is an increase in current and a slight decrease in speed. When the load is reduced to half of the rated torque, the current decreases accordingly. In both scenarios, the DC bus voltages remain stable, indicating that the speed remains stable in steady-state conditions. However, during the transient period, there are small overshoots and undershoots in speed for a brief duration.

8. Conclusion

In this study, a solar PV array-based BLDC motor-driven E-rickshaw with a Landsman converter was analyzed for its startup, dynamic, and steady-state characteristics through both modeling and real-world application of the developed system. The use of a Landsman converter eliminates the need for external filters and helps reduce oscillations in the module current, which typically arise from snubber components. The hybrid PV-wind system under investigation is designed to completely self-supply the load during operation. Simulation results from MATLAB SIMULINK demonstrated the excellent performance of the proposed system. The results showed that both the solar and wind generators could supply the load with the required energy and charge the battery. The sensor-less control method calculates commutation points based on the voltage level and DC bus voltage. Any imbalance or variation in the bus voltage leads to erroneous commutation, significant current ripple, and a distorted current profile. The proposed approach significantly reduces these current ripples, ensuring smoother and more reliable sensor-less commutation. Additionally, this method minimizes interference pulses by estimating the commutation time using freewheeling signals. The MPPT performance of the upgraded Landsman converter has been greatly enhanced. Furthermore, the system's energy efficiency is significantly improved due to regenerative braking. Therefore, the proposed approach proves to be practical and suitable for BLDC vehicle applications, particularly in low-cost light electric vehicles.

9. References

1. Saha B, Singh B. Solar PV integration to e-rickshaw with regenerative braking and sensorless control. In: Proceedings of the IEEE 17th India Council International Conference; 2020 Dec; p. 1-6.
2. Yang L, Zhu ZQ, Bin H, Zhang Z, Gong L. Virtual third harmonic back EMF-based sensorless drive for high-speed BLDC motors considering machine parameter asymmetries. IEEE Transactions on Industrial Applications. 2021 Jan; 57(1):306-315.
3. Zhou X, Chen X, Zeng F, Tang J. Fast commutation instant shift correction method for sensorless coreless BLDC motor based on terminal voltage information. IEEE Transactions on Power Electronics. 2017 Dec; 32(12):9460-9472.
4. Acarnley PP, Watson JF. Review of position-sensorless operation of brushless permanent-magnet machines. IEEE Transactions on Industrial Electronics. 2006 Apr; 53(2):352-362.
5. Damodharan P, Vasudevan K. Sensorless brushless DC motor drive based on the zero-crossing detection of back electromotive force (EMF) from the line voltage difference. IEEE Transactions on Energy Conversion. 2010 Sep; 25(3):661-668.
6. Chen S, Liu G, Zhu L. Sensorless control strategy of a 315kW high-speed BLDC motor based on a speed-independent flux linkage function. IEEE Transactions on Industrial Electronics. 2017 Nov; 64(11):8607-8617.
7. Chen S, Zhou X, Bai G, Wang K, Zhu L. Adaptive commutation error compensation strategy based on a flux linkage function for sensorless brushless DC motor drives in a wide speed range. IEEE Transactions on Power Electronics. 2018 May; 33(5):3752-3764.
8. Bierhoff MH. A general PLL-type algorithm for speed sensorless control of electrical drives. IEEE Transactions on Industrial Electronics. 2017 Dec; 64(12):9253-9260.
9. Zhou X, Chen X, Peng C, Zhou Y. High-performance non-salient sensorless BLDC motor control strategy from standstill to high speed. IEEE Transactions on Industrial Informatics. 2018 Oct; 14(10):4365-4375.
10. Lee AC, Fan CJ, Chen GH. Current integral method for fine commutation tuning of sensorless brushless DC motor. IEEE Transactions on Power Electronics. 2017 Dec; 32(12):9249-9266.
11. Gu C, Wang X, Shi X, Deng Z. A PLL-based novel commutation correction strategy for a high-speed brushless DC motor sensorless drive system. IEEE Transactions on Industrial Electronics. 2018 May; 65(5):3752-3762.
12. Tan B, Wang X, Zhao D, Shen K, Zhao J, Ding X. A lag angle compensation strategy of phase current for high-speed BLDC motors. IEEE Access. 2019;7:9566-9574.
13. Lee DM, Lee WC. Analysis of relationship between abnormal current and position detection error in sensorless controller for interior permanent-magnet brushless DC motors. IEEE Transactions on Magnetics. 2008 Aug; 44(8):2074-2081.
14. Li H, Zheng S, Ren H. Self-correction of commutation point for high-speed sensorless BLDC motor with low inductance and non-ideal back EMF. IEEE Transactions on Power Electronics. 2017 Jan; 32(1):642-651.
15. Peng H, Wang J, Shen W, Shi D, Huang Y. Controllable regenerative braking process for hybrid battery-ultracapacitor electric drive systems. IET Power Electronics. 2018 Dec; 11(15):2507-2514.
16. Yang MJ, Jhou HL, Ma BY, Shyu KK. A cost-effective method of electric brake with energy regeneration for electric vehicles. IEEE Transactions on Industrial Electronics. 2009 Jun; 56(6):2203-2212.
17. Fazeli A, Zeinali M, Khajepour A. Application of adaptive sliding mode control for regenerative braking torque control. IEEE/ASME Transactions on Mechatronics. 2012 Aug; 17(4):745-755.
18. Zhang X, Wang Y, Liu G, Yuan X. Robust regenerative charging control based on T-S fuzzy sliding-mode approach for advanced electric vehicle. IEEE Transactions on Transportation Electrification. 2016 Mar; 2(1):52-65.
19. Bobba PB, Rajagopal KR. Compact regenerative braking scheme for a PM BLDC motor driven electric two-wheeler. In: Proceedings of the Joint International Conference on Power Electronics, Drives, and Energy Systems; 2010 Dec; p. 1-5.
20. Wyczalek F, Wang T. Regenerative braking concepts

for electric vehicles—A primer. In: International Congress & Expo, SAE Technical Paper 920648; 1992.
21. Cao Y, Shi T, Yan Y, Li X, Xia C. Braking torque control strategy for brushless DC motor with a non-inductive hybrid energy storage topology. IEEE Transactions on Power Electronics. 2020 Aug; 35(8):8417-8428.
22. Naseri F, Farjah E, Ghanbari T. An efficient regenerative braking system based on battery/supercapacitor for electric, hybrid and plug-in hybrid electric vehicles with BLDC motor. IEEE Transactions on Vehicular Technology. 2017 May; 66(5):3724-3738.
23. Li P, Sun W, Shen JX. Flux observer model for sensorless control of PMBLDC motor with amperage. IEEE Transactions on Industrial Applications. 2019 Mar; 55(2):1272-1279.
24. Ogasawara S, Akagi H. An approach to position sensorless drive for brushless DC motors. IEEE Transactions on Industrial Applications. 1991 Oct; 27(5):928-933.
25. Shao J. An improved microcontroller-based sensorless brushless DC (BLDC) motor drive for automotive applications. IEEE Transactions on Industrial Applications. 2006 Sep; 42(5):1216-1221.
26. Saha B, Singh B. An economical approach for solar PV-battery based e-rickshaw with regenerative braking using sensorless BLDC motor drive. In: Proceedings of the IEEE International Conference on Power Electronics, Drives, and Energy Systems; 2020 Dec; p. 1-6.